Theoretical Investigation of the Biogenetic Pathway for Formation of Antibacterial Indole Alkaloids from *Voacanga africana*

Esra N. Soysal, Volkan Fındık, Burcu Dedeoglu, Viktorya Aviyente, and Dean J. Tantillo*

Read Online

ACCESS | Metrics & More | Article Recommendations | Supporting Information

prohibitively high barrier for biological conditions
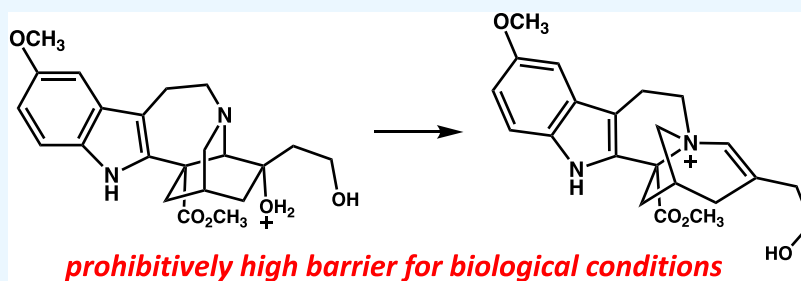
ABSTRACT: The energetic viability of the previously proposed biogenetic pathway for the formation of two unique monoterpenoid indole alkaloids, voacafricine A and B, which are present in the fruits of *Voacanga africana*, was investigated using density functional theory computations. The results of these calculations indicate that not only is the previously suggested pathway not energetically viable but also that an alternative biosynthetic precursor is likely.

INTRODUCTION

Antibiotic resistance has contributed to an increasing interest in the development of plant-based antibiotics. Plant-derived natural products have been used in traditional medicine since ancient times. For example, *Voacanga africana* (Apocynaceae) is a flowering small tropical tree native to West Africa. Its root bark is used to treat diarrhea in Kinshasa,[1] while its stem bark has been used in the treatment of leprosy, diarrhea, ulcers, generalized edema, and microbial infections in Côte d'Ivoire, Ghana, Cameroon, and Congo.[2,3] Additionally, in Cameroon, the fruits, leaf extracts, and seed extracts are used to treat orchitis, gonorrhea, and tooth decay, respectively.[4−8] Most of the applications of *V. africana* are linked to its antimicrobial properties.[9,10] Pharmacological studies have found that the main bioactive compounds that are responsible for its success as a traditional medicine are monoterpenoid indole alkaloids (MIAs).[11] In a recent study,[12] the fruits of *V. africana* were investigated and two MIAs, called voacafricine A and voacafricine B (Scheme 1), were isolated and shown to possess antibacterial activity against *Staphylococcus aureus* and *Salmonella typhi* bacteria. This study suggested a plausible biogenetic pathway (Scheme 1) involving 19-epi-voacristine as a precursor. This 6/5/7/6/6 pentacycle is a major indole alkaloid present in *V. africana*.[13] Curious about the geometric constraints these polycyclic structures would impose on a rearrangement such as that proposed, we evaluated the energetic viability of the proposed process using density functional theory calculations to determine which elementary steps, if any, would require enzymatic intervention.[14−16]

In the proposed pathway,[12] dehydration of 19-epi-voacristine generates 4,20-didehydro-voacangine (Scheme 1). The introduction of hydroxyl groups to the C-18 and 20 positions of 4,20-didehydro-voacangine forms a diol intermediate, which could be protonated to form **A** in anticipation of water loss. Loss of water and cleavage of the C-16−C-21 bond leads to proposed intermediate **B**, which could reclose (via N-4 attack on C-16) to form intermediate **C**. The conversion of **A** to **C** was our focus. Intermediate **C** could then be transformed to voacafricine A via epoxidation, intramolecular nucleophilic substitution, and ester hydrolysis and voacafricine B via deoxygenation.

Computational Methods. All calculations were performed with Gaussian16.[17] Geometry optimizations were performed using mPW1PW91/6-31+G(d,p), a level of theory that has been used to model many carbocation rearrangements.[18] Calculations were performed in the gas phase, water, and chloroform. Calculations with implicit solvents were performed using the Polarizable Continuum Model (PCM).[19] Continuum dielectric environments corresponding to two solvents were used: water ($\varepsilon = 78.36$), a very polar solvent, and chloroform ($\varepsilon = 4.71$), a nonpolar solvent with a

Scheme 1. Proposed Biogenetic Pathway to Voacafricine A and B Starting From 19-epi-voacristine
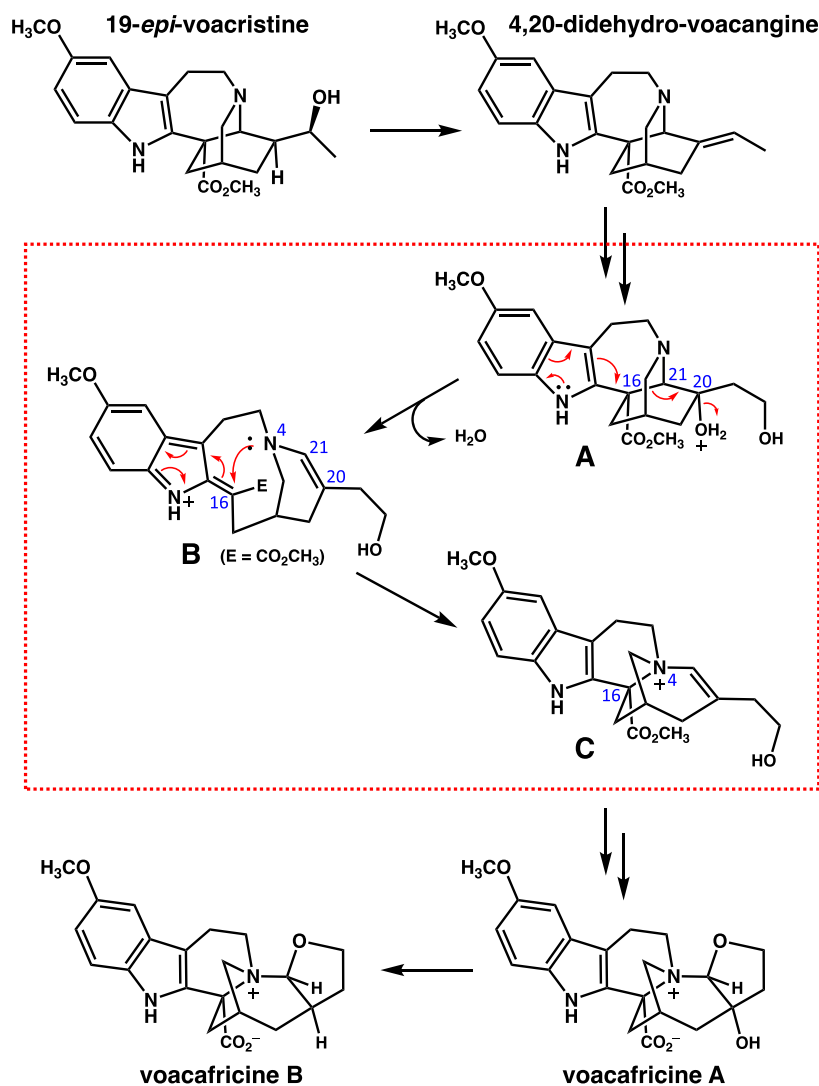
dielectric constant that falls within the range of estimates for enzyme active sites.[20] Structures also were optimized at the B3LYP-D3(BJ)/6-311+G(d,p)[21] and M06-2X/6-311+G-(d,p)[22] levels to compare geometries and relative energies. For key transition structures (TSs), which were confirmed to have single imaginary frequencies, intrinsic reaction coordinates (IRCs) were computed to verify the minima to which they are connected.[23] All energies given are free energies at room temperature, except those in the IRC plots, which are electronic energies. CylView2.0[24] was used to generate three-dimensional molecular images.

RESULTS AND DISCUSSION

The computed free energy profile for the conversion of **A** to **C** in water (see the SI for results in the gas phase and chloroform) is given in Figure 1, and TS geometries are shown in Figure 2. On the basis of our results, the conversion of **A** to **B** cannot occur in a single step, but rather it would involve three discrete chemical steps.

First, the loss of water is facilitated by a nearby tertiary amine, which displaces the water to form an aziridinium ion (**A1**). The A → **A1** reaction is predicted to have a low barrier (∼10 kcal/mol). Polycyclic natural product-derived aziridi-

nium ions have been described previously.[25] Shown in Figure 3 is the computed structure of intermediate **A1**. All four N−C distances in **A1** are close to each other and are in the range expected for typical N−C single bonds (ranging from 1.47 to 1.53 Å). While some C−N−C bond angles in **A1** are distorted, this structure does not show the geometric features expected for a nonclassical ion and instead resembles a classical aziridinium ion, similar to other polycyclic natural product-derived aziridium ions.[25]

Second, cleavage of the C-16−C-21 bond coupled to a 1,2-shift of C-16 to C-20 and cleavage of the C-20−N-4 bond leads to **A2**. To characterize the synchronicity of these bond-forming/breaking events, the IRC for the **A1** → **A2** reaction (Figure 4) was analyzed in detail (Figure 5).[26−29] Before [**TS2**]‡ is reached, the N-4−C-20 bond breaks, leading to a TSS that resembles a hyperconjugated but classical alkyl cation (Figures 2 and 4). Subsequently, a 1,2-alkyl shift process ensues as the C-16−C-21 and C-16−C-20 bonds break and form synchronously. The resulting cation is in conjugation with the N-4 lone pair, leading to a shortening of the N-4−C-21 bond. The **A1** → **A2** reaction is predicted to have a barrier of ∼30 kcal/mol, which, based on the analysis above, appears to arise primarily from C−N bond cleavage. The magnitude of this barrier indicates that if this pathway is followed, enzyme-
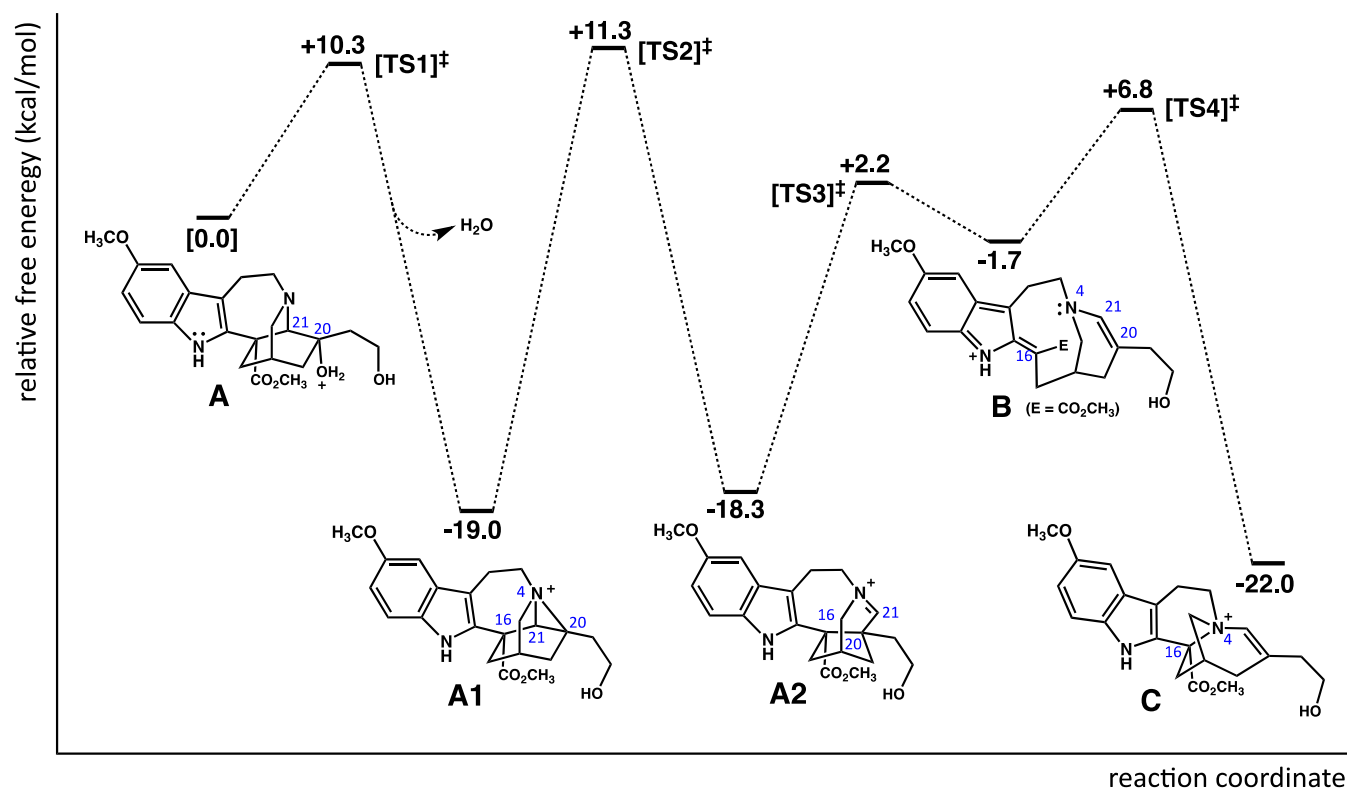
Figure 1. Relative free energies (PCM(water)-mPW1PW91/6-31+G(d,p), kcal/mol) of species involved in the **A → B → C** pathway.
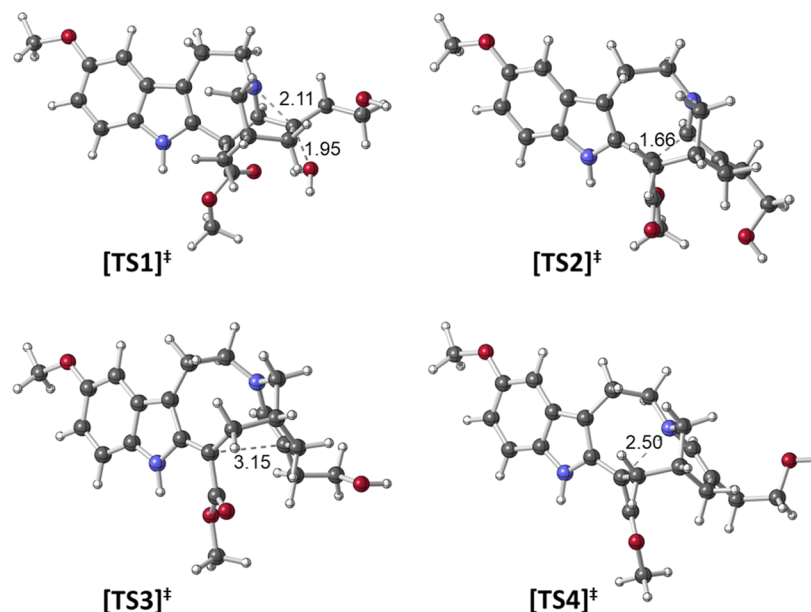

Figure 2. Geometries of optimized TSs from Figure 1. Selected distances shown on the three-dimensional molecular images are in Å.

induced barrier lowering would be required, either by selective stabilization of [**TS2**]‡, selective destabilization of **A1**, or both.

Third, cleavage of the C-16−C-20 bond, promoted by π-electron donation from the indole, generates intermediate **B**. This step is predicted to be endergonic and to have a barrier of ∼20 kcal/mol.

Conversion of **B** to **C** is predicted to proceed directly, as suggested previously, with a low barrier (∼7 kcal/mol). However, the overall conversion of **A1** to [**TS4**]‡ is predicted

to involve a barrier of ∼26 kcal/mol, again pointing to the necessity of enzymatic intervention.

Thus, there is a problem with the **A → C** pathway: two barriers >25 kcal/mol are encountered en route to **C**. Reducing these through enzymatic intervention is not impossible but is a lot to ask of Nature. Nonetheless, we examined this possibility using "theozyme" calculations.[30,31] Since the **A1 → A2** barrier was predicted to be the largest, we focused on its reduction. We examined complexes of **A1** and [**TS2**]‡ with one or two water molecules (also models of hydroxyl-containing enzyme
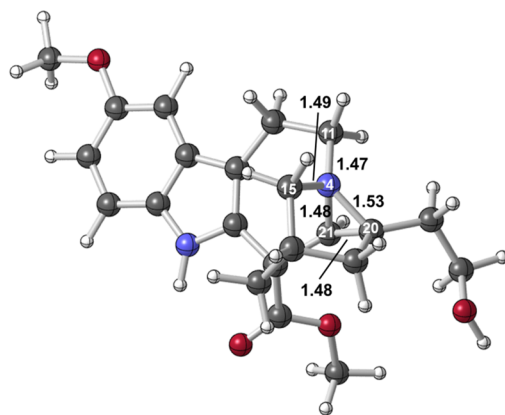
Bond angles: C11-N4-C20 = 131.2°, C11-N4-C21 = 113.0°, C20-N4-C21 = 58.7°, C20-N4-C15 = 107.7°, C21-N4-C15 = 116.9°, C11-N4-C15 = 116.5°

Figure 3. Computed structure of intermediate **A1** [mPW1PW91/6-31+G(d,p)]. Selected distances are provided in Å.
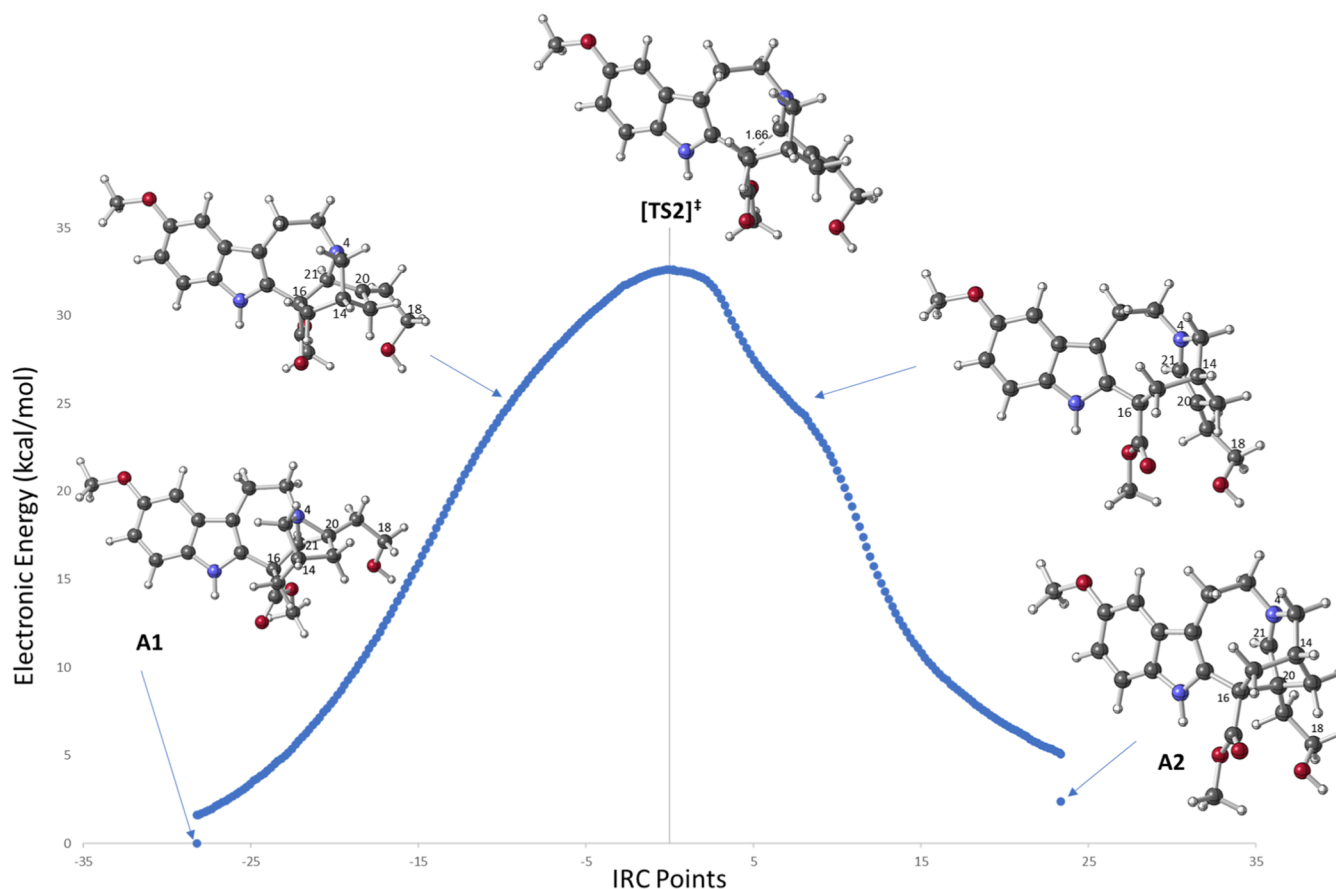

Figure 4. IRC plot obtained [PCM(water)-mPW1PW91/6-31+G(d,p)] for the formation of intermediate **A2**. Energies for IRC points are electronic energies in kcal/mol relative to the reactant.

sidechains), formate (a simple model of Asp and Glu), trifluoroacetate (a model of Asp and Glu that accounts for pK_a lowering in an enzyme), and benzene (a model of aromatic enzyme sidechains). In none of these cases did the predicted **A1** → **A2** barrier drop below 24 kcal/mol (see the Supporting Information for details). While these results do not definitively rule out the possibility of extreme enzymatic barrier lowering, we consider it unlikely. In addition, alternative mechanisms connecting **A** to **C** were considered, but none were found to have lower barriers than that discussed above (see the

Supporting Information for details). It is notable, however, that natural products with skeletons similar to that of **B** but derived from different precursors have been described.[32]

■ CONCLUSIONS

Using DFT calculations, a proposed rearrangement mechanism involved in the biosynthesis of voacafricine A and B was examined and found not to be energetically viable. Additional calculations addressing the potential for lowering the barrier for this process through selective transition state stabilization
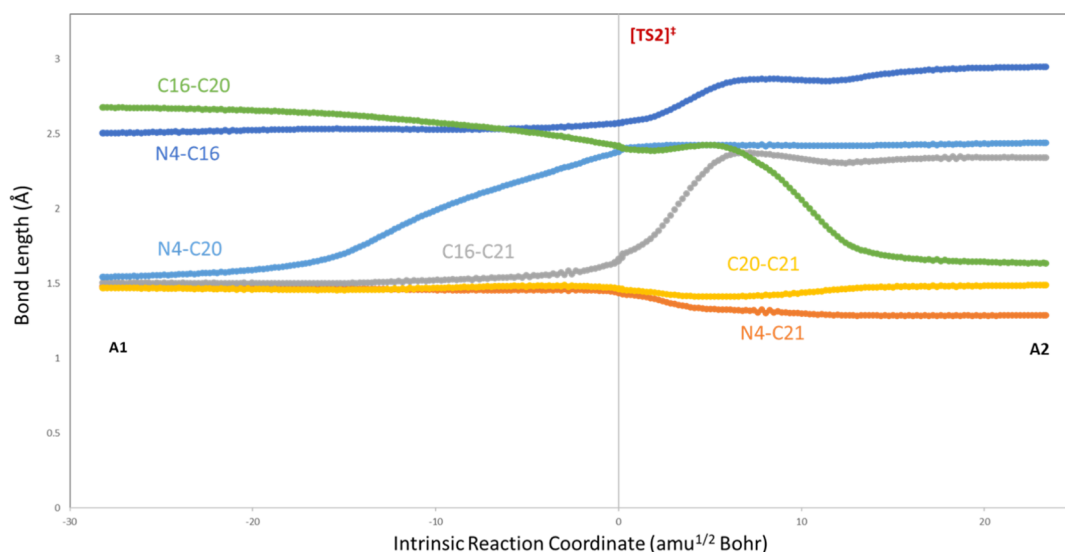
Figure 5. Evolution of selected interatomic distances as the reaction progresses along the IRC (Figure 4).

by an enzyme did not reveal an array of potential active site groups that would lower the barrier into a biologically reasonable range. Given these results, and our inability to find an alternative path connecting the same reactants and products, we suggest that alternatives to structures **A** and/or **C** be considered.

ASSOCIATED CONTENT

Supporting Information

The Supporting Information is available free of charge at https://pubs.acs.org/doi/10.1021/acsomega.2c04591.

> Optimized structures of the intermediates, geometry of optimized transition state structure 5, relative free energies of species involved in the C → D pathway, computed energies of the intermediates and TSSs, IRC plots for the formation of intermediates and evolution of the key bond lengths as the reaction progresses along the IRC, calculations with theozymes, other trials to find an alternative pathway, and all computed structures (https://iochem-bd.bsc.es/browse/review-collection/100/216406/83e73067f39b82b021143601) (PDF)

AUTHOR INFORMATION

Corresponding Author

Dean J. Tantillo − *Department of Chemistry, University of California-Davis, Davis, California 95616, United States;* orcid.org/0000-0002-2992-8844; Email: djtantillo@ucdavis.edu

Authors

Esra N. Soysal − *Department of Chemistry, University of California-Davis, Davis, California 95616, United States; School of Chemistry, University of Edinburgh, Edinburgh EH9 3FJ, United Kingdom;* orcid.org/0000-0002-4920-4720

Volkan Fındık − *Université de Lorraine, CNRS, LPCT, Nancy F54000, France; Department of Chemistry, Faculty of Arts and Sciences, Marmara University, Istanbul 34722, Turkey*

Burcu Dedeoglu − *Department of Chemistry, Gebze Technical University, Gebze 41400 Kocaeli, Turkey;* orcid.org/0000-0001-9504-2913

Viktorya Aviyente − *Department of Chemistry, Bogazici University, Bebek 34342 Istanbul, Turkey;* orcid.org/0000-0001-9430-4096

Complete contact information is available at:
https://pubs.acs.org/10.1021/acsomega.2c04591

Notes

The authors declare no competing financial interest.

ACKNOWLEDGMENTS

ABBREVIATIONS

MIA, monoterpenoid indole alkaloid; DFT, density functional theory; PCM, Polarizable Continuum Model; TS, transition structure; IRC, intrinsic reaction coordinate

REFERENCES

(1) Tona, L.; Kambu, K.; Mesia, K.; Cimanga, K.; Apers, S.; De Bruyne, T.; Pieters, L.; Totté, J.; Vlietinck, A. J. Biological screening of traditional preparations from some medicinal plants used as antidiarrhoeal in Kinshasa, Congo. *Phytomedicine* **1999**, *6*, 59−66.

(2) Liu, X.; Yanga, D.; Liu, J.; Ren, N. Synthesis and acetylcholinesterase inhibitory activities of tabersonine derivatives. *Phytochem. Lett.* **2015**, *14*, 17−22.

(3) Chen, H. M.; Yang, Y. T.; Li, H. X.; Cao, Z. X.; Dan, X. M.; Mei, L.; Guo, D. L.; Song, C. X.; Dai, Y.; Hu, J.; Deng, Y. Cytotoxic monoterpenoid indole alkaloids isolated from the barks of Voacanga africana Staph. *Nat. Prod. Res.* **2016**, *30*, 1144−1149.

(4) Tan, P. V.; Nyasse, B. Anti-ulcer compound from Voacanga africana with possible histamine H2 receptor blocking activity. *Phytomedicine* **2000**, *7*, 509−515.

(5) Tan, P. V.; Penlap, V. B.; Nyasse, B.; Nguemo, J. D. B. Anti-ulcer actions of the bark methanol extract of Voacanga africana in different experimental ulcer models in rats. *J. Ethnopharmacol.* **2000**, *73*, 423−428.

(6) Jiofack, T.; Fokunang, C.; Kemeuze, V.; Fongnzossie, E.; Tsabang, N.; Nkuinkeu, R.; Mapongmetsem, P. M.; Nkongmeneck, B. A. Ethnobotany and Phytopharmacopoea of the South-West Ethno-ecological Region of Cameroon. *J. Med. Plants Resour.* **2008**, *2*, 197−206.

(7) Hussain, H.; Hussain, J.; Al-Harrasi, A.; Green, I. R. Chemistry and biology of the genus Voacanga. *Pharm. Biol.* **2012**, *50*, 1183−1193.

(8) Kitajima, M.; Iwai, M.; Kogure, N.; Kikura-Hanajiri, R.; Goda, Y.; Takayama, H. Aspidosperma-aspidosperma-type bisindole alkaloids from Voacanga africana. *Tetrahedron* **2013**, *69*, 796−801.

(9) Glick, S. D.; Gallagher, C. A.; Hough, L. B.; Rossman, K. L.; Maisonneuve, I. M. Differential effects of ibogaine pretreatment on brain levels of morphine and (+)-amphetamine. *Brain Res.* **1992**, *588*, 173−176.

(10) Popik, P.; Layer, R. T.; Skolnick, P. 100 Years of Ibogaine: Neurochemical and Pharmacological Actions of a Putative Anti-addictive Drug. *Pharmacol. Rev.* **1995**, *47*, 235−253.

(11) Federici, E.; Palazzino, G.; Nicoletti, M.; Galeffi, C. Antiplasmodial activity of the alkaloids of Peschiera fuchsiaefolia. *Planta Med.* **2000**, *66*, 93.

(12) Ding, C. F.; Ma, H. X.; Yang, J.; Qin, X. J.; Njateng, G. S. S.; Yu, H. F.; Wei, X.; Liu, Y. P.; Huang, W. Y.; Yang, Z. F.; Wang, X. H.; Luo, X. D. Antibacterial indole alkaloids with complex heterocycles from Voacanga africana. *Org. Lett.* **2018**, *20*, 2702−2706.

(13) Perera, P.; Samuelsson, G.; van Beek, T. A.; Verpoorte, R. Tertiary indole alkaloids from leaves of Tabernaemontana dichotoma. *Planta Med.* **1983**, *47*, 148−150.

(14) Tantillo, D. J. Importance of Inherent Substrate Reactivity in Enzyme-Promoted Carbocation Cyclization/Rearrangements. *Angew Chem. Int. Ed. Engl.* **2017**, *56*, 10040−10045.

(15) Painter, P. P.; Pemberton, R. P.; Wong, B. M.; Ho, K. C.; Tantillo, D. J. The Viability of Nitrone−Alkene (3 + 2) Cyclo-additions in Alkaloid Biosynthesis. *J. Org. Chem.* **2014**, *79*, 432−435.

(16) Krenske, E. H.; Patel, A.; Houk, K. N. Does Nature Click? Theoretical Prediction of an Enzyme-Catalyzed Transannular 1,3-Dipolar Cycloaddition in the Biosynthesis of Lycojaponicumins A and B. *J. Am. Chem. Soc.* **2013**, *135*, 17638−17642.

(17) Frisch, M. J.; Trucks, G. W.; Schlegel, H. B.; Scuseria, G. E.; Robb, M. A.; Cheeseman, J. R.; Scalmani, G.; Barone, V.; Petersson, G. A.; Nakatsuji, H.; Li, X.; Caricato, M.; Marenich, A. V.; Bloino, J.; Janesko, B. G.; Gomperts, R.; Mennucci, B.; Hratchian, H. P.; Ortiz, J. V.; Izmaylov, A. F.; Sonnenberg, J. L.; Williams-Young, D.; Ding, F.; Lipparini, F.; Egidi, F.; Goings, J.; Peng, B.; Petrone, A.; Henderson, T.; Ranasinghe, D.; Zakrzewski, V. G.; Gao, J.; Rega, N.; Zheng, G.; Liang, W.; Hada, M.; Ehara, M.; Toyota, K.; Fukuda, R.; Hasegawa, J.; Ishida, M.; Nakajima, T.; Honda, Y.; Kitao, O.; Nakai, H.; Vreven, T.; Throssell, K.; Montgomery, J.; Peralta, J. E.; Ogliaro, F.; Bearpark, M. J.; Heyd, J. J.; Brothers, E. N.; Kudin, K. N.; Staroverov, V. N.; Keith, T. A.; Kobayashi, R.; Normand, J.; Raghavachari, K.; Rendell, A. P.; Burant, J. C.; Iyengar, S. S.; Tomasi, J.; Cossi, M.; Millam, J. M.; Klene, M.; Adamo, C.; Cammi, R.; Ochterski, J. W.; Martin, R. L.; Morokuma, K.; Farkas, O.; Foresman, J. B.; Fox, D. J. *Gaussian16, Revision C.01*; Gaussian, Inc.: Wallingford CT, 2016.

(18) Tantillo, D. J. Biosynthesis via carbocations: theoretical studies on terpene formation. *Nat. Prod. Rep.* **2011**, *28*, 1035−1053.

(19) Herbert, J. M.; Lange, A. W. *Many- Body Effects and Electrostatics in Multi-Scale Computations of Biomolecules*, Cui, Q., Markus, M.; Pengyu, R., Eds., Jenny Stanford Publishing, 1st edn., 2016, pp. 363−416.

(20) Simonson, T.; Brooks, C. L. Charge Screening and the Dielectric Constant of Proteins: Insights from Molecular Dynamics. *J. Am. Chem. Soc.* **1996**, *118*, 8452−8458.

(21) (a) Becke, A. D. A new mixing of Hartree-Fock and local density functional theories. *J. Chem. Phys.* **1993**, *98*, 1372−1377. (b) Grimme, S.; Antony, J.; Ehrlich, S.; Krieg, H. A consistent and accurate *ab initio* parametrization of density functional dispersion correction (DFT-D) for the 94 elements H-Pu. *J. Chem. Phys.* **2010**, *132*, 154104.

(22) Zhao, Y.; Truhlar, D. G. The M06 suite of density functionals for main group thermochemistry, thermochemical kinetics, non-covalent interactions, excited states, and transition elements: Two new functionals and systematic testing of four M06-class functionals and 12 other function. *Theor. Chem. Acc.* **2008**, *120*, 215−241.

(23) (a) Fukui, K. The Path of Chemical Reactions - The IRC Approach. *Acc. Chem. Res.* **1981**, *14*, 363−368. (b) Gonzalez, C.; Schlegel, H. B. Reaction path following in mass-weighted internal coordinates. *J. Phys. Chem.* **1990**, *94*, 5523−5527. (c) Maeda, S.; Harabuchi, Y.; Ono, Y.; Taketsugu, T.; Morokuma, K. Intrinsic Reaction Coordinate: Calculation, Bifurcation, and Automated Search. *Int. J. Quantum Chem.* **2015**, *115*, 258−269.

(24) Legault, C. Y. *CYLview 2.0*; Université de Sherbrooke, 2020.

(25) Lodewyk, M. W.; Tantillo, D. J. Nonclassical ammonium ions as intermediates in cinchona alkaloid rearrangements? *Chirality* **2020**, *32*, 484−488.

(26) Hong, Y. J.; Ponec, R.; Tantillo, D. J. Changes in charge distribution, molecular volume, accessible surface area and electronic structure along the reaction coordinate for a carbocationic triple shift rearrangement of relevance to diterpene biosynthesis. *J. Phys. Chem. A* **2012**, *116*, 8902−8909.

(27) Tantillo, D. J. Recent excursions to the borderlands between the realms of concerted and stepwise: Carbocation cascades in natural products biosynthesis. *J. Phys. Org. Chem.* **2008**, *21*, 561−570.

(28) Houk, K. N.; Gonzalez, J.; Li, Y. Pericyclic Reaction Transition States: Passions and Punctilios, 1935-1995. *Acc. Chem. Res.* **1995**, *28*, 81−90.

(29) Dewar, M. J. S.; Jie, C. Mechanisms of Pericyclic Reactions: The Role of Quantitative Theory in the Study of Reaction Mechanisms. *Acc. Chem. Res.* **1992**, *25*, 537−543.

(30) Tantillo, D. J.; Jiangang, J.; Houk, K. N. Theozymes and compuzymes: theoretical models for biological catalysis. *Curr. Opin. Chem. Biol.* **1998**, *2*, 743−750.

(31) Tantillo, D. J.; Houk, K. N. *Simulating Concepts in Chemistry*; Wiley: Weinheim, Germany, 2000, pp 79−88.

(32) Caputi, L.; Franke, J.; Farrow, S. C.; Chung, K.; Payne, R. M. E.; Nguyen, T.-D.; Dang, T.-T. T.; Soares Teto Carqueijeiro, I. S. T.; Koudounas, K.; Dugé de Bernonville, T. D.; Ameyaw, B.; Jones, D. M.; Vieira, I. J. C.; Courdavault, V.; O'Connor, S. E. Missing enzymes in the biosynthesis of the anticancer drug vinblastine in Madagascar periwinkle. *Science* **2018**, *360*, 1235−1239.